Synthesis and Characterization of Ordered Arrays of Topological Defects in Mesoporous Silica Films

Hugh W. Hillhouse, Jan W. van Egmond,† and Michael Tsapatsis*

Department of Chemical Engineering, University of Massachusetts, Amherst, Massachusetts 01003

Jonathon C. Hanson and John Z. Larese

Department of Chemistry, Brookhaven National Laboratory, Upton, New York 11973

Received May 25, 2000. Revised Manuscript Received August 1, 2000

Defects are commonly found throughout crystalline solids and often have a pronounced effect on mechanical, optical, chemical, and transport properties.[1] Liquid-crystalline materials also contain defects resulting in topologies where the director field is undefined at a point or on a curve at the defect core.[2] In both the crystalline and liquid-crystalline state, defects typically disrupt long-range order, rendering the material isotropic at large length scales. Acid synthesis of mesoporous silica proceeds through a liquid-crystalline stage[3] in which defects determine the channel orientation of the resulting porous material. Previously, hexagonal phase mesoporous silica films have been grown with channels dominantly oriented parallel to the substrate.[4−6] Here, we report that ordered arrays of topological defects can be generated leading to mesoporous silica films with long-range orientation and rotational order with approximately half of the channels oriented perpendicular to the substrate by growing the films epitaxially on a crystalline substrate in a shear flow field. Two-dimensional X-ray diffraction patterns recorded from films grown on mica are "single-crystal-like," exhibiting 6-fold symmetry that is rotationally invariant over the entire film.

Introduction

The synthesis of surfactant-templated mesoporous silica was first reported[7] in 1992. This discovery and subsequent investigations of the formation mechanism[8] opened up a new methodology for nanostructured material synthesis and generated a surge of interest in the areas of catalysis,[9] adsorption, dye lasers,[10] and inclusion chemistry.[11] The hexagonal phase of mesostructured silica spontaneously self-assembles under a wide range of conditions from solutions containing amphiphilic molecules and silica precursors. Condensation reactions cross-link the silica in the assembly to create an inorganic framework. After the silica framework is formed, the amphiphiles can be removed by calcination or solvent extraction. The result is a material consisting of a periodic hexagonal array of mesoscopic pores with a uniform pore size determined by the choice of amphiphile used during synthesis. Thin films of these materials have also been synthesized and may one day be used as membrane nanotubular reactors, novel membrane separators, or in fundamental studies of confined growth and transport. However, successful application of these and other mesostructured materials hinges on discovering methods for controlling the orientation of the mesostructure over macroscopic distances. Producing films of these materials with extended orientational order is challenging because the hexagonal phase possesses plane-group symmetry, $p6mm$, in the $a-b$ plane but lacks periodicity along the c direction (the direction of the pores) as shown in Figure 1. As a result, the hexagonal array of one-dimensional pores may bend to form curved morphologies, disrupting long-range orientational order.

When the hexagonal phase is synthesized under acidic conditions, the morphology of homogeneously nucleated particles is dominated by defined structures[12] that are known to grow in a layer-by-layer fashion[6] from a

† Current address: Union Carbide Corporation, South Charleston, WV 25303.

(1) Kittel, C. *Introduction to Solid State Physics*, 7 ed.; John Wiley & Sons: New York, 1996.
(2) Chandrasekhar, S. *Liquid Crystals*, 2nd ed.; Cambridge University Press: Cambridge, 1992.
(3) Ozin, G. A.; Kresge, C. T.; Yang, H. Nucleation, growth and form of mesoporous silica: role of defects and a language of shape. In *Mesoporous Molecular Sieves*; Bonneviot, L., Beland, F., Danumah, C., Giasson, S., Kaliaguine, S., Eds.; Elsevier: Amsterdam, 1998; pp 119−127.
(4) Aksay, I. A.; Trau, M.; Manne, S.; Honma, I.; Yao, N.; Zhou, L.; Fenter, P.; Eisenberger, P. M.; Gruner, S. M. *Science* **1996**, *273*, 892−898.
(5) Yang, H.; Kuperman, A.; Coombs, N.; Mamiche-Afara, S.; Ozin, G. A. *Nature* **1996**, *379*, 703−705.
(6) Hillhouse, H. W.; Okubo, T.; Egmond, J. W. v.; Tsapatsis, M. *Chem. Mater.* **1997**, *9*, 1505−1507.
(7) Kresge, C. T.; Leonnowicz, M. E.; Roth, W. J.; Vartuli, J. C.; Beck, J. S. *Nature* **1992**, *359*, 710.
(8) Monnier, A.; Schuth, F.; Huo, Q.; Kumar, D.; Margolese, D.; Maxwell, R. S.; Stucky, G. D.; Krishnamurty, M.; Petroff, P.; Firouzi, A.; Janicke, M.; Chmelka, B. F. *Science* **1993**, *261*, 1299−1303.
(9) Ying, J. Y.; Mehnert, C. P.; Wong, M. S. *Angew Chem. Int. Ed. Engl.* **1999**, *38*, 56−77.
(10) Yang, P.; Wirnsberger, G.; Huang, H. C.; Cordero, S. R.; McGehee, M. D.; Scott, B.; Deng, T.; Whitesides, G. M.; Chmelka, B. F.; Buratto, S. K.; Stucky, G. D. *Science* **2000**, *287*, 465−467.
(11) Moller, K.; Bein, T. *Chem. Mater.* **1998**, *10*, 2950−2963.
(12) Yang, H.; Coombs, N.; Ozin, G. A. *Nature* **1997**, *386*, 692−695.

10.1021/cm000425k CCC: $19.00
Published on Web 09/23/2000

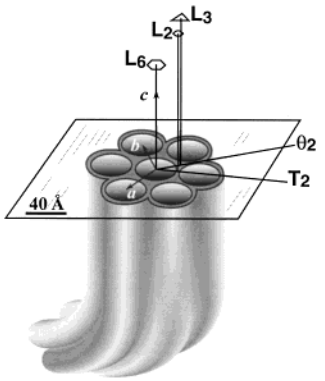

Figure 1. Schematic of the mesostructure of the *p*6*mm* hexagonal phase showing its symmetry elements. Note the lack of periodicity in the *c* direction, allowing the channels to bend.

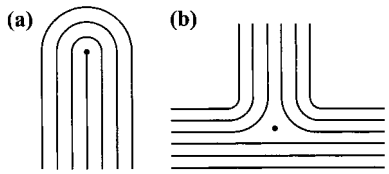

Figure 2. Schematic showing configurations of a director field (the *c* direction in the hexagonal phase of mesoporous silica) for two types of line defects: (a) a $+\pi$ disclination and (b) a $-\pi$ disclination.

cooperatively assembled silica-surfactant seed.[3] Before the assembly becomes rigid due to silica cross-linking, the labile mesostructure is liquid-crystal-like and may form defects similar to those in liquid crystals. Topological similarities between the mesostructure and liquid-crystalline phases are apparent from the textures observed in polarized optical microscopy images which bear strong resemblance to those observed from liquid crystals. These images reveal that the liquid-crystal-like topology is preserved during silica cross-linking and removal of the organic template. Theoretical investigations by Bouligand[13] have identified energetically favorable defects and defect pairs that may occur in hexagonal nonsmectic liquid-crystalline mesophases, and recent experimental results show strong similarities between these predicted topologies and the observed morphologies of mesoporous silica.[14] Defects were first observed in mesoporous silica[15] from transmission electron microscopy images where longitudinal edge dislocations, hybrid (edge-screw) dislocation dipoles, $+\pi$ disclinations, and disclination quadrupoles were identified. Under acid synthesis conditions, many of the observed particle morphologies are now understood to originate from combinations of such topological defects.[3] These disclinations (line defects) are rotations of the director field (the pore orientation) about a given axis. Schematics for two types of disclinations are shown in Figure 2. It should be noted that disclinations about the transverse axes (T_2 and θ_2) alter the pore orientation, while disclinations about the longitudinal axes (L_6, L_3, and L_2) alter the rotational configuration of the array.

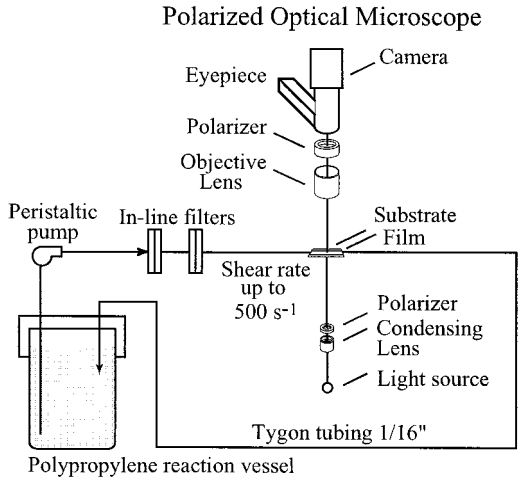

Figure 3. Experimental apparatus used to synthesize mesostructured silica films on a flat substrate in an applied flow field.

Due to the lack of periodicity along the *c* direction (see Figure 1) of the mesostructure and the presence of topological defects, mesostructured silica particles, grown in solution, contain pores that may sample any orientation. However, films synthesized at the air−water interface exhibit two-dimensional (2D) U-shaped, S-shaped, and "fingerprint" curved morphologies in the plane of the interface.[16] These morphologies are generated since the mesophase nucleates with the *c* direction parallel to the interface. Disclinations occur about transverse axes that are perpendicular to the plane of the interface, creating films that have pores parallel to the interface but that sample all orientations in the plane. The pore orientation can further be confined to 1D by epitaxially growing the mesophase on a single crystal substrate. Mesostructured silica films have previously been grown on mica,[5,4,17] graphite,[18] and silicon surfaces.[19] In each case, the mesostructure was correlated to the crystalline lattice of the substrate with the channels oriented parallel to the surface. In the current study, by growing the films epitaxially on high-grade mica substrates and adjusting mass-transfer rates by applying a flow field during growth, we find that topological defects occur that are correlated to the crystal lattice of the substrate. This results in films with defined channel orientation and rotational configuration with a fraction of the channels oriented perpendicular to the substrate.

Experimental Section

Synthesis. Films were synthesized at room temperature from a precursor mixture as previously reported.[17] The mixture was transferred to a polypropylene beaker and peristaltically pumped through a continuous flow cell over a freshly cleaved mica substrate where the reacting solution flows with a small periodic oscillation in the volumetric flow rate; see Figure 3. The flow cell consists of a 1 mm^2 horizontal channel where

(13) Bouligand, Y. *J. Phys.* **1980**, *41*, 1297−1306.
(14) Yang, H.; Ozin, G. A.; Kresge, C. T. *Adv. Mater.* **1998**, *10*, 883−887.
(15) Feng, J.; Huo, Q.; Petroff, P. M.; Stucky, G. D. *Appl. Phys. Lett.* **1997**, *71*, 1887−1889.
(16) Yang, H.; Coombs, N.; Sokolov, I.; Ozin, G. A. *J. Mater. Chem.* **1997**, *7*, 1755−1761.
(17) Yang, H.; Coombs, N.; Ozin, G. A. *J. Mater. Chem.* **1998**, *8*, 1205−1211.
(18) Yang, H.; Coombs, N.; Sokolov, I.; Ozin, G. A. *J. Mater. Chem.* **1997**, *7*, 1285−1290.
(19) Miyata, H.; Kuroda, K. *J. Am. Chem. Soc.* **1999**, *121*, 7618−7624.

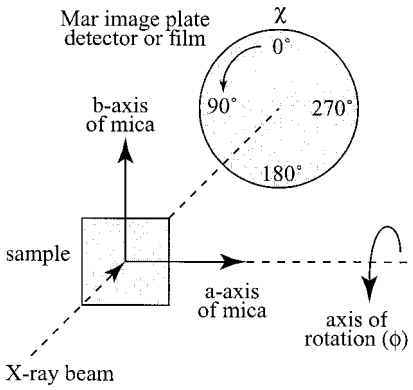

Figure 4. Schematic showing the configuration used to collect transmission X-ray diffraction patterns.

the mica substrate constitutes the top surface. The films were grown from 6 h to 4 days in flow fields with average shear rates from 50 to 500 s^{-1}. Grade V-4 muscovite substrates were obtained from SPI Supplies (www.2spi.com), 25 × 25 mm^2 and 0.26 mm thick. The surfactant template was removed as previously reported[17] by vacuum dehydration at 100 °C and calcination in air at 450 °C.

X-ray Diffraction. The synthesized films were analyzed on beam-line X7B of the National Synchrotron Light Source at Brookhaven National Laboratory. Two-dimensional X-ray diffraction patterns were collected in transmission geometry with the beam perpendicular to the substrate using a MAR 345 image plate detector, Figure 4. The camera length, beam diameter, and radiation wavelength were 425 mm, 0.5 mm, and 1.5659 Å, respectively. Laue-projection photographs were collected on Kodak direct-exposure film by orienting the substrate normal to an unfiltered Cu X-ray beam in an evacuated chamber at a camera length of 54 mm (same geometry as that shown in Figure 4).

Microscopy. Scanning electron microscopy (SEM) images were obtained using a JEOL 100 CX microscope operated at an accelerating voltage of 20 kV. The samples were coated with gold using a Polaron E5100 sputter coater prior to imaging. Transmission electron microscopy (TEM) images were obtained from thin sections (ca. 800−1200 Å) by embedding the films in LR White acrylic resin (London Resin Company) and sectioning with a Sorvall Porter-Blum MT-2B ultra-microtome using a Diatome diamond knife. The films were sputter-coated with gold prior to embedding in resin to help identify the top surface of the film in TEM images. The film cross sections were then imaged using a JEOL 100CX microscope operated at an accelerating voltage of 100 kV. Polarized optical microscopy (POM) images were obtained both in situ and after synthesis in transmission mode with the sample between crossed polarizers on an Olympus BX60 optical microscope.

Results and Discussion

Muscovite has a natural cleavage plane along the crystallographic $a-b$ plane, allowing well-defined crystal surfaces to be prepared easily. Various polytypes of muscovite are formed by specific stacking sequences of these planes. Natural mica contains predominantly the $2M_1$ polytype with smaller amounts of the 3T and 1M polytypes. The $2M_1$ polytype is composed of alternating sheets that are offset to one another by 60° in the $a-b$ plane. Low-quality mica has a disordered stacking sequence and is labeled as the 1d structure. Since there are likely many atomic steps on the surface of the substrate after cleavage, it is necessary that high-quality mica of a defined polytype be used such that the resulting epitaxial overgrowth is oriented macroscopically.

Structure. The crystal structure of the $2M_1$ polytype of muscovite is reported in the monoclinic space group $C2/c$ with lattice constants $a = 5.201$, $b = 8.697$, and $c = 20.058$ Å, and $\alpha = 90°$, $\beta = 95.8°$, and $\gamma = 90°$ by Bailey.[20] In reciprocal space, the a^*-c^* plane is the only mirror plane in the centered monoclinic unit cell of muscovite. This creates mirror symmetry across the projection of the a axis in the Laue photograph shown in Figure 5a and allows the crystal perfection and orientation in the lab frame to be determined easily.[21] Once the substrate orientation is known, the diffraction spots from the substrate may easily be indexed with monochromatic radiation. The epitaxial overgrowth of the hexagonal mesophase on muscovite is seen from 2D synchrotron X-ray data in Figure 5b. The low-angle diffraction spots are from the mesostructured film and exhibit approximate 6-fold symmetry. Note the azimuthal alignment of the diffraction spots from the muscovite substrate with the diffraction spots from the mesostructure.

The d spacings of the observed diffraction spots confirm the presence of the $p6mm$ hexagonal phase of mesostructured silica indexed with lattice constants $a = b = 48.95$ Å, c is undefined, and $\alpha = 90°$, $\beta = 90°$, and $\gamma = 120°$. The observed diffraction pattern from the mesostructure could possibly be generated from either a single orientation that has channels perpendicular to the substrate, several discrete orientations with channels parallel to the substrate, or a combination of both. The later is found to be the case, and these results are distinguished by collecting diffraction patterns after rotation of the substrate and film in the X-ray beam. After a 30° rotation about the ϕ axis, it is observed that the peak at $\chi = 0°$ ($d = 42.4$ Å) labeled $010_\perp$ and the peak at $\chi = 30°$ ($d = 24.5$ Å) labeled 110_u are absent while a peak at $\chi = 30°$ ($d = 42.4$ Å) labeled 100_u has appeared (also note the lack of appearance of a peak at $\chi = 0°$ with $d = 24.5$ Å); see Figure 6. These extinction characteristics indicate that the diffraction from the peak labeled $010_\perp$ originates from a region with the c direction perpendicular to the substrate while the diffraction from the peaks labeled 100_u and 110_u originate from a region with the c direction parallel to the substrate and rotationally oriented with the T_2 axis also parallel to the substrate. Note that reflections at azimuthal angles other than $\chi = 0°$ or 180° are not rotated by ϕ but by a corrected $\phi' = [90° - \text{acos}(\sin\phi \cos\chi)]$. As a result, reflections will not extinguish until the angle ϕ' becomes larger than the mosaic spread of the diffracting planes.

The fact the sample does not probe all rotational configurations (about the L_6 axis of the mesostructure) allows one to isolate the orientation of the channels by the above "single-crystal" X-ray analysis. The key is that a region of channels oriented parallel to the substrate (for a given rotational configuration about the L_6 axis) will produce diffraction spots at the d_{100}, d_{110}, and d_{200} spacings the along same angle χ when the substrate is rotated about the ϕ axis. By rotating the substrate/sample about an axis parallel to the X-ray beam and

(20) Bailey, S. W. Classification and structure of the micas. In *Micas: Reviews in Minerology 13*; Bailey, S. W., Ed.; BookCrafters: Chelsea, 1984.

(21) Amoros, J. L.; Buerger, M. J.; Amoros, M. C. d. *The Laue Method*; Academic Press: New York, 1975.

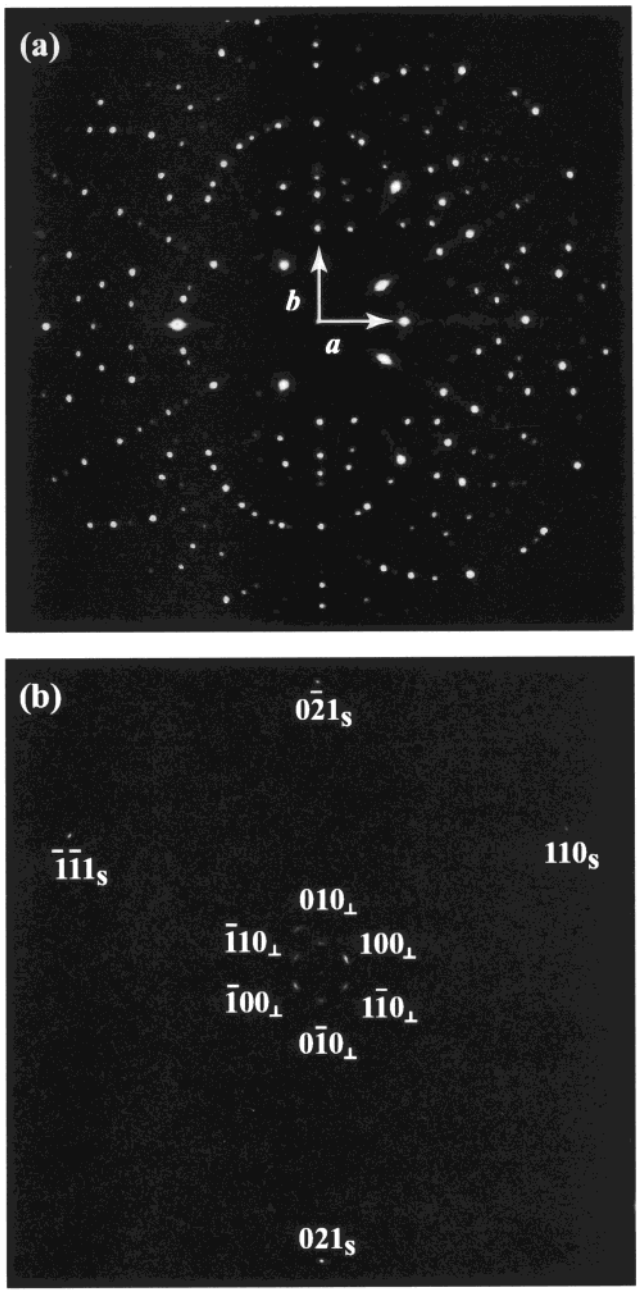

Figure 5. Two-dimensional transmission X-ray diffraction patterns showing epitaxial growth of the hexagonal mesophase on a muscovite substrate. (a) Diffraction pattern from a polychromatic source (unfiltered Cu) at short camera length (54 mm). In reciprocal space, the a^*-c^* plane of the $2M_1$ polytype of muscovite is the only mirror plane in the centered monoclinic unit cell of the muscovite. This creates mirror symmetry across the projection of the a axis and allows the crystal orientation of the substrate in the lab frame to be determined easily. (b) Synchrotron data using 1.5659 Å wavelength at longer camera length (425 mm) showing the epitaxial alignment between the hexagonal mesophase and the muscovite substrate. The diffraction peaks from the substrate are indexed with the $2M_1$ polytype and are labeled as hkl_s. The lower angle scattering is from the mesophase, and the peaks are indexed in the plane group $p6mm$ from a perpendicularly orientated phase and are labeled $hkl_\perp$.

repeating the ϕ axis rotation, all of the diffraction peaks may be indexed, as shown in Figure 6. The a axis of the perpendicular oriented hexagonal mesophase is found to be co-aligned with the a axis of the muscovite substrate, as seen in Figure 5. Approximately half of

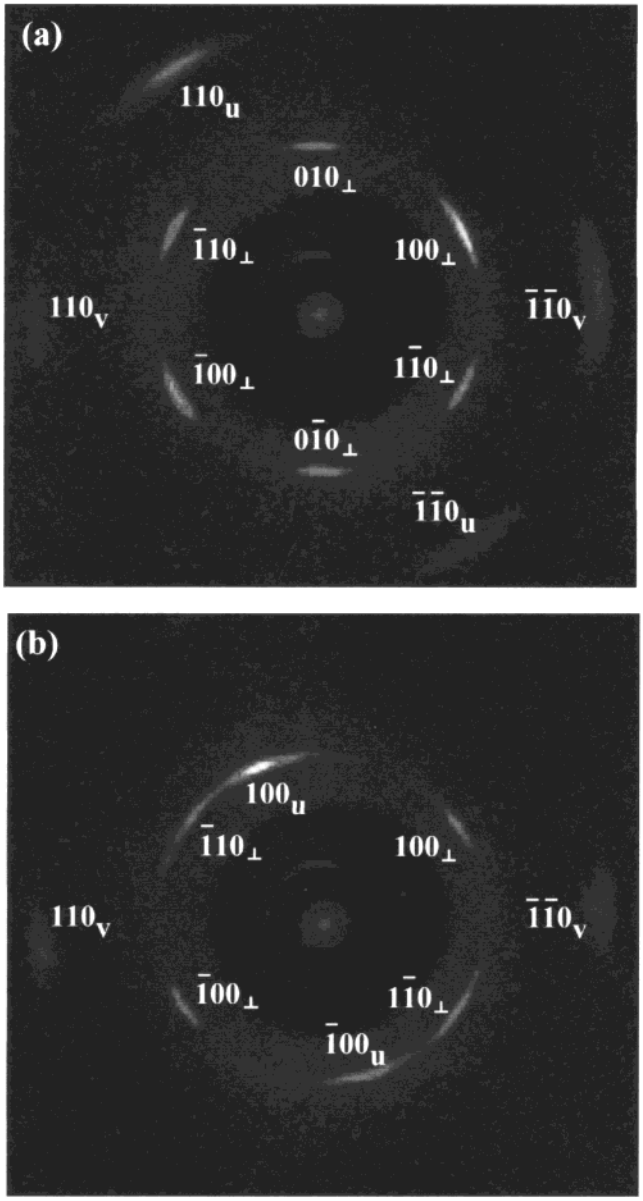

Figure 6. Two-dimensional X-ray diffraction patterns of the sample rotated about the ϕ axis (see Figure 4). (a) Enlargement of the low-angle region of 2D X-ray diffraction pattern shown in Figure 5 for $\phi = 0°$. Six reflections from the mesophase are found at a spacing of 42.4 Å and display 6-fold symmetry. These peaks are indexed as the (100), (−100), (010), (0−10), (−110), and (1−10) reflections from a mesophase oriented with the pores perpendicular to the substrate. Weaker peaks at 24.5 and 21.2 Å (the spacings of the (110) and (200) reflections) may be indexed to regions of the mesophase with the pores oriented parallel to the substrate. (b) Diffraction pattern for $\phi = 30°$ showing that the observed intensity at $d_{110} = 24.5$ Å and $\chi = 30°$ (110_u from Figure 6a) is due to diffraction from regions with the c direction parallel to the substrate and rotationally oriented with the 100 face parallel to the substrate. Another orientation with the c-direction parallel to the substrate is also seen, and intensities from these orientations are labeled hkl_u and hkl_v.

the channels were found oriented normal to the substrate as determined by comparing the relative diffracted intensities of the orientations. The lattice misfit of the overgrowth was determined to be 4.6%, defined as $(a_{\text{mesophase}} - 9a_{\text{muscovite}})/9a_{\text{muscovite}} \times 100$. In addition, three mesophase orientations (separated by 60°) are found with channels parallel to the substrate and

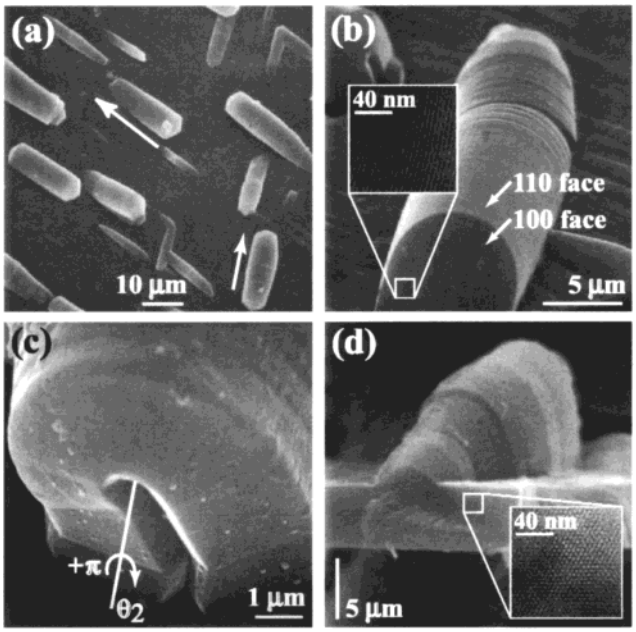

Figure 7. Electron micrographs of the synthesized mesostructured film showing the morphology of structures epitaxially grown on mica substrates in an applied flow field. (a) Top-view SEM image showing two discrete orientations of elongated structures. Arrows indicate the *c* direction of the mesostructure in regions of the film beside the elongated structures, as determined by POM and TEM. (b) Side-view SEM image with a TEM image inset from a region of the film similar to that indicated by the box. The TEM image shows channels oriented perpendicular to the substrate. (c) Side-view SEM image showing the location of a $+\pi$ disclination about the transverse 2-fold axis, θ_2. (d) Cross-sectional SEM image with a TEM image inset from a region of the film similar to that indicated by the box showing a hexagonal array of pores oriented parallel to the substrate.

rotationally oriented with the T_2 axis also parallel to the substrate. These three orientation are due to the chemical equivalence of these directions on the surface lattice of the muscovite at the cleavage plane.[4] The diffraction data shows that the relative populations of these three horizontal orientations are unbalanced with approximately a 20:5:1 ratio, resulting possibly from the applied flow field. After synthesis, the framework and orientation are found to be stable upon template removal by calcination and thus create a mesoporous framework of the structure described above.

The morphology of the films synthesized in the applied laminar flow field is shown in SEM images in Figure 7. TEM analysis of microtomed cross-sections of the film confirms the above X-ray analysis and shows that within the horseshoe-like structures the channels are oriented perpendicular to the substrate. TEM images also show that the vertical orientation of the channels extends below the surface of the film. It is noted that the channels of the mesostructure are tangent to the observed curved surfaces. In addition, these horseshoe-like structures are elongated and oriented in three discrete directions (only two are observed in Figure 7a) correlated to the underlying crystalline mica lattice. POM and TEM data shows that the *c* direction of the mesostructure in the surrounding film is coincident with the direction of elongation.

A possible topology of some of the elongated structures is shown schematically in Figure 8 and is seen to result

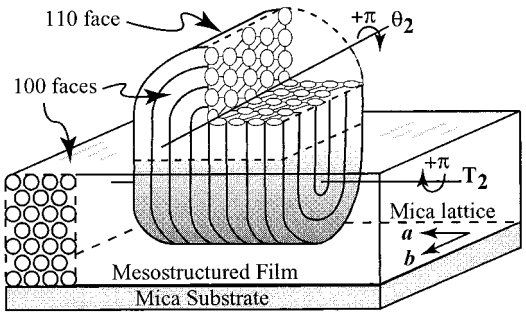

Figure 8. Topology embedded in the mesoporous film that may be generated by an orthogonal pair of $+\pi$ disclinations. A disclination along the T_2 axis combined with one along the θ_2 axes generates the dual-horseshoe structure shown. Note that for this topology the 110 crystal face (next-nearest-neighbor arrangement) is exposed on the top curved surface while the 100 crystal face (nearest-neighbor arrangement) is present on the bottom. Differing growth rates of these crystal faces exposed to the nutrient solution could lead to the anisotropy of the structures observed in Figure 7a.

from the orthogonal combination of two $+\pi$ disclinations. The topology from this defect pair was previously predicted by Bouligand[13] and later observed in homogeneously nucleated mesostructured silica by Yang et al.[14] Also, there are other possible defect combinations that may produce similar structures such as an orthogonal pair of $-\pi$ and $+\pi$ disclinations.

Formation Mechanism. Several possible formation mechanisms are suggested by the observed experimental data. However, it is important to note that films, grown under identical conditions on amorphous glass substrates, also display $+\pi$, $-\pi$, and $+2\pi$ disclinations. However, the growth remains confined to 2D, and the resulting channel orientation is always parallel to substrate. This suggests that the morphologies observed here on crystalline substrates are due to the epitaxial nature of the growth. One possibility is that homogeneously nucleated particles that already embody the defect core may adhere epitaxially to the growing film surface. However, particles from the bulk solution observed by SEM after synthesis have a wide variety of morphologies and defect cores while the elongated structures in the film are all very similar to one another. Alternatively, defects in the film may be produced dynamically during growth due to reaction-induced stresses or epitaxial mismatch. The film growth appears to be mass-transfer limited, and POM images show that the films grown in a flow field have a much smaller domain size than identical synthesis chemistry in quiescent solution, as seen in Figure 9. This suggests that the effect of the flow field is to increase mass-transfer and, as a result, also increase the number density of nuclei on the surface and the film growth rate. POM images obtained in situ are limited to a resolution of approximately 0.5 μm and, as such, cannot be used to image the nucleation event. When the film is thick enough to be resolved, the defects are already present.

Conclusions

In the current study, epitaxial growth in the plane of the substrate creates a film with the *c* direction oriented in three discrete directions parallel to the substrate while subsequent topological defects force the *c* direction

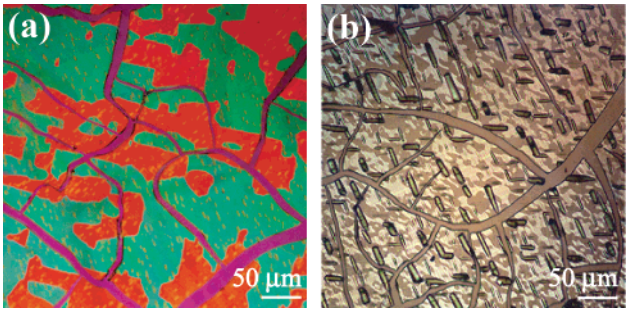

Figure 9. POM images at 200× magnification of mesostructured films grown on mica. Since the assembled liquid crystal (and resulting mesoporous material) is birefringent, domains of differing orientation in the plane of the substrate are observed as different colors or shades (the sample in part a has a thicker substrate that produces color in the image from interference between the layers of the muscovite). (a) POM image from a film grown without an applied flow field. The purple is the substrate while the red and green colors indicate a domain of a single orientation. (b)) POM image from a film grown in an applied flow field with an approximate shear rate of 100 s^{-1}. The domains of single orientation are seen as light or dark patches. The images show that the domain size of a given orientation is much smaller for that synthesis in an applied flow field.

to grow perpendicular to the substrate. The rotational configuration of the channels about the L_6 axis is preserved over the 2.5 cm dimension of substrate and the 5 μm thickness of the film and results in the observation of 6-fold symmetry in transmission X-ray diffraction patterns. This rotational confinement has hitherto not been identified. The films have high mechanical integrity and may be removed from the substrate after calcination. It is noted that the mesopores oriented perpendicular to the substrate are capped due to the topology. However, plasma ion etching or other related approaches may potentially be used to expose the channel openings.

Acknowledgment. Support for this work was provided by NETI and NSF (CAREER Award CTS/9624613). X-ray analysis at Brookhaven National Laboratory was supported under Contract DE-AC02-98CH-10886 with the U.S. Department of Energy by its Divisions of Chemical and Material Sciences, Office of Basic Energy Sciences. M.T. acknowledges support from a David & Lucile Packard Fellowship in Science and Engineering and a Camille & Henry Dreyfus Teacher−Scholar Award.

CM000425K